Global, Hybrid, MIMO Implementation of the Algorithm of Mode Isolation

M. S. Allen, and J. H. Ginsberg
The G. W. Woodruff School of Mechanical Engineering
Georgia Institute of Technology
Atlanta, GA 30332-0405

October 20, 2004

Abstract

The Algorithm of Mode Isolation (AMI) employs a strategy in which modes are sequentially identified and subtracted from a set of FRFs. Their natural frequencies, damping ratios and mode vectors are then refined through an iterative procedure. This contrasts conventional multi-degree-of-freedom (MDOF) identification algorithms, most of which attempt to identify all of the modes of a system simultaneously. This paper presents a hybrid multi-input-multi-output (MIMO) implementation of the algorithm of mode isolation that improves the performance of AMI for systems with very close or weakly excited modes. The algorithmic steps are amenable to semi-automatic identification, and many FRFs can be processed efficiently without concern for ill-conditioning. The performance of the algorithm is demonstrated on noise contaminated analytical response data from two systems having close modes, one of which has localized modes while the other has globally responsive modes. The results are compared with other popular algorithms.

Nomenclature

$H_{jP}(\omega)$	FRF for displacement j due to excitation P	$\{\phi_r\}$	displacement portion of rth mode vector (Normalized)
H_{c}	Composite FRF	$\{q\}$	Generalized coordinates
H_{cn}	Condensed FRF (Nyquist Plots)	w	Transverse displacement
$[A_r]$	Modal residue matrix for the rth mode	θ	Torsional rotation
		N_i	Number of inputs
λ_r	rth eigenvalue	N_o	Number of outputs
ω_r	rth natural frequency	α	Peak selection parameter
ζ_r	rth modal damping ratio	SR	Singular Value Ratio
ω	Drive frequency	RF	Reduction Factor

1 Introduction

As applications of Experimental Modal Analysis (EMA) expand, the need for accurate algorithms capable of handling large data sets with low signal to noise ratios is apparent. While the efforts of the past few decades have resulted in several capable new algorithms, a number of difficulties remain. These difficulties are most apparent in situations where high accuracy is important, such as condition monitoring.

The objectives in experimental modal analysis differ from those in general system identification, in that the goal is meaningful modes of vibration, rather than matching of input and output data. The conventional approach to modal parameter identification involves applying a multi-degree-of-freedom (MDOF) identification algorithm to estimate all of the natural frequencies, damping ratios and mode shapes of the system simultaneously. In many problems, a number of computational modes are identified along with the true modes of the system. The common approach in such a situation is to apply the MDOF algorithm at a number of model orders, and then plot the resulting

eigenvalues on a stabilization diagram. (A stabilization diagram charts the eigenvalues as a function of the model order.) Modes that have similar modal parameters over a range of model orders are assumed to be true modes, while the remaining modes are discarded. One difficulty with this approach is that it might be difficult to discern computational modes from true modes on the stabilization diagram [1], [2]. Also, there can be significant variation in the modal parameters estimated from one model order to the next, so that even when the true modes can be identified on a stabilization diagram, it may be difficult to tell which model order(s) results in accurate estimates of their modal parameters. Furthermore even if an algorithm yields modal parameters that are consistent from one model order to the next, it might be that there is a constant bias error relative to the true modal parameters. For example, the authors found this to occur when applying the SSI algorithm to noise contaminated analytical data in [3].

The Algorithm of Mode Isolation (AMI) operates in a manner that obviates the need for a stabilization diagram, resulting in a fast, accurate, and intuitive approach to modal parameter estimation. Previous comparisons of AMI to some standard MDOF algorithms [4], [5], [6] have shown that AMI gives accurate results when applied to synthetic data for a few prototypical analytical systems. The present work is a global, MIMO extension of AMI, in which FRFs for all response points are processed simultaneously. The algorithm assures that rank-one residue matrices are found for each mode, so that a consistent modal model is always obtained.

The Algorithm of Mode Isolation (AMI) is based upon the recognition that the FRF data to be fit is a superposition of individual modal contributions. AMI identifies each mode individually, and then subtracts its contribution from the data. Modes are subtracted from the data set until only noise remains, thereby identifying the model order as the number of modes subtracted before the data is reduced to noise. An iterative procedure is then used to refine the initial estimate in order to account for overlapping contributions of adjacent modes. The use of low order fits limited to data near the resonant peaks results in a computationally efficient algorithm. The algorithm also provides a self-correcting check that the initial identification of the number of contributory modes is correct.

The general concept of mode isolation was first suggested by Kirshenboim [7], and seems to have been implemented as part of the Modent package [8]. The first detailed investigation of the methodology was presented by Drexel and Ginsberg [4], in which it was dubbed the Mode Isolation Algorithm (MIA), and then subsequently the Algorithm of Mode Isolation (AMI). While the references to the methodology are sparse in the literature, a few researchers have reported trying similar procedures in communications with the authors. Recently, Yin and Duhamel [9] reported using a similar SISO technique, although they used finite difference formulas to identify the modal parameters whereas AMI uses a least-squares fit. Improvements to the AMI algorithm presented by Drexel and Ginsberg and the results of test problems are documented in [5], [6], [10], [11], [12], [13], [14], and [15].

The global, SIMO implementation of AMI can encounter difficulty when applied to systems having close modes. The subtraction stage is based upon the assumption that SDOF fits to FRF data in a narrow band around the peaks will give an adequate approximation of the individual modes of the system. If the resonant peaks for two modes having comparable magnitude merge, an SDOF fit to the merged peak does not give a good approximation of either mode. In such a situation one might subtract countless modes from a narrow frequency band without reducing the data to noise. On the other hand, if poor approximations of closely spaced modes are accepted in the subtraction phase, a divergent situation may result when the modal parameters are refined in the isolation phase.

This paper addresses these difficulties by allowing for either a single or multi-mode fit to each set of peak data. The algorithm considers each peak in the FRF data, and applies either an SDOF fit if a single mode is dominant, or an MDOF fit if multiple close modes are dominant. The procedure represents a hybrid approach because it combines the conventional simultaneous, MDOF viewpoint with AMI's concept of sequentially subtracting modal contributions from the data set. The next section presents the details of the hybrid MIMO implementation of AMI. In section 3 the proposed algorithm is applied to noise-contaminated analytical response data from a frame structure having a pair of localized modes with close natural frequencies. Section 4 presents the application of MIMO-AMI to analytical data from a simply-supported, rectangular plate with globally active modes having very close natural frequencies. Section 5 presents some conclusions. The application of MIMO-AMI to experimental data is presented in a companion paper [16].

2 Hybrid, MIMO Implementation of AMI

The discussion herein will focus on the global, hybrid, MIMO implementation of AMI. Differences between this and the prior global, SIMO implementation presented in [6] will be highlighted. The data analyzed in MIMO-AMI

consists of the frequency response of N_o outputs or measurement degrees-of-freedom (DOF) to harmonic forces at N_i input degrees of freedom denoted $P_1 ... P_{N_i}$. (The input and output degrees of freedom could be interchanged by exploiting reciprocity.) It is assumed that the system dynamics can be represented by the familiar second order matrix differential equation

$$[M]\{\ddot{q}\} + [C]\{\dot{q}\} + [K]\{q\} = \{F\} \tag{1}$$

where $\{q\}$, $[M]$, $[C]$, and $[K]$ are the generalized coordinate vector, and symmetric mass, damping and stiffness matrices respectively each of dimensions $N \times N$. A MIMO data set consists of the standard collection of FRFs describing the response at each of the outputs to harmonic forces applied at each of the inputs individually. Specifically, the kth data set is a column vector of dimensions $(N_o \times 1)$ at each frequency, describing the response at all measurement points due to a force vector $\{F\}$ that is zero everywhere except the P_kth generalized coordinate or drive point, where a unit force is applied. A column of responses is collected for $k = 1..N_i$, resulting in the frequency response function matrix $[H_P(\omega)]$, of dimensions $(N_o \times N_i)$ at each frequency point. A number of well established methods exist for collecting such a data set [17], [18]. The frequency response function matrix is related to the state space modal properties by

$$[H(\omega)] = \sum_{r=1}^{N} \left(\frac{[A_r]}{i\omega - \lambda_r} + \frac{[A_r^*]}{i\omega - \lambda_r^*} \right) \tag{2}$$
$$[A_r] = \lambda_r \{\phi_r\} \left\lfloor \phi_{P_1,r} \ldots \phi_{P_{N_i},r} \right\rfloor$$

where λ_r and $\{\phi_r\}$ are the complex eigenvalue and the displacement portion of the complex normalized eigenvector of the rth mode of vibration and $()^*$ denotes a complex conjugate. (See [19] or [15] for a more detailed discussion of the state space eigenvalue problem.) The notation $\phi_{P_k,r}$ signifies the P_kth element of the displacement portion of the rth mode vector, where P_k is the index for the kth input or drive point. The residue matrix for mode r is an $N_o \times N_i$ matrix denoted $[A_r]$. The eigenvalue is related to the "undamped" natural frequency ω_r and damping ratio ζ_r by $\lambda_r = -\zeta_r \omega_r \pm \omega_r \left(1 - \zeta_r^2\right)^{1/2}$. It is important to note, that because the residue matrix is formed as the product of a column and a row vector, it has a rank of unity. In a companion paper [16] a modified definition of the residue matrix was used that is valid for non-reciprocal systems.

In practice, the variables that are measured are not necessarily the generalized coordinates $\{q\}$ of the system. For example, only a finite number of measurements are taken from continuous systems, which have an infinite number of degrees of freedom. Similarly, when a Ritz model is used the physical displacements that are measured are linear combinations of the underlying Ritz series coefficients. These situations can be represented by defining measurement degrees of freedom $\{y\}$ such that

$$\{y\} = [B]\{q\} \tag{3}$$

where $[B]$ can be non-square. If the system is also excited at the same measurement degrees of freedom $\{y\}$ or some subset thereof, the forces $\{F\}$, associated with the generalized coordinates, are related to the forces $\{u\}$ by

$$\{F\} = [B]^T \{u\}. \tag{4}$$

Taking the Fourier transforms of these definitions and substituting into eq. (2) results in an FRF matrix $[H_y(\omega)]$, in terms of the measurement degrees of freedom, satisfying

$$\{Y(\omega)\} = [H_y(\omega)]\{U(\omega)\} \tag{5}$$
$$[H_y(\omega)] = [B][H(\omega)][B]^T \tag{6}$$

where $\{Y(\omega)\}$ and $\{U(\omega)\}$ denote the Fourier transform of the responses at the measurement degrees of freedom and the forces applied at the measurement degrees of freedom respectively. From this, it is evident that the same number of modes appears in any given frequency band, regardless of which set of FRFs are processed. Furthermore, the pole-residue model in eq. (2) remains valid if the eigenvectors observed at the measurement degrees of freedom $\{u_r\} = [B]^T \{\phi_r\}$ replace the eigenvectors in terms of the generalized coordinates $\{\phi_r\}$.

2.1 Subtraction Stage

AMI is a two-stage process, beginning with the subtraction stage in which modes are sequentially identified and

subtracted from the experimental data. The algorithm starts by considering the highest peak of the composite FRF, where the composite FRF is defined as the average of the magnitude of the FRFs for all response points as follows,

$$H_c(\omega) = composite([H(\omega)]) = \frac{1}{N_o N_i} \sum_{k=1}^{N_i} \sum_{j=1}^{N_o} |H_{jP_k}(\omega)| . \tag{7}$$

At each peak, the number of modes contributing to the response and estimates for their parameters are determined. In the SISO and SIMO versions of AMI, modes were identified and subtracted one at a time. The hybrid MIMO-AMI algorithm preserves the idea of subtracting modal contributions from the data. However, it allows for the possibility that more than one mode might contribute significantly to a peak as a consequence of proximity of natural frequencies, in which case groups of modes are simultaneously subtracted from the data.

To begin identifying and subtracting modes, data in a frequency interval surrounding the highest peak of the composite FRF is selected. In the most basic approach a user could manually set frequency bands around peaks of interest in the composite FRF, but such an approach requires an expert user and significant user interaction. The authors have had good success with an automatic procedure, in which the frequency band is set by including only data for which the composite FRF is greater than a specified fraction of the peak value. This fraction is called the peak selection parameter α, so the selection criterion is

$$H_c(\omega) > \alpha * \max(H_c(\omega)) \tag{8}$$

For example, $\alpha = 0.707$ corresponds to using all points within the half-power bandwidth. Setting $\alpha = 0.5$ has worked well for many problems. For some systems, visual inspection might reveal that the frequency points selected using $\alpha = 0.5$ are not concentrated around the peak of interest. This may occur due to high noise, high modal density, or significant out of band modal contributions. In such cases a larger peak selection parameter might be needed, resulting in fewer frequency points being selected.

For each set of peak data the number of modes present and estimates of the parameters of those modes will be determined. Initially, the algorithm tries a single-degree of freedom fit on the peak data using a "common-denominator" MIMO algorithm. The specific algorithm used is the SIMO algorithm presented in [6], in which the FRFs for all $N_i N_o$ input-output combinations are processed globally, as if they resulted from a SIMO experiment with $N_i N_o$ outputs. This algorithm yields the eigenvalue for the mode active at the peak, and the corresponding $N_o \times N_i$ residue matrix denoted $[A_{\text{fit}}]$. Evaluation of certain metrics, combined with a visual comparison of the composite FRF and a composite recontructed using the identified modes, reveals the number of modes active at that peak. If the evaluation determines that a single mode is present, the original residue matrix is processed to find a rank-one residue $[A_{\text{fit,R1}}]$ (see eq. (11).) If multiple modes are detected at the resonant peak, a MIMO, MDOF fitting algorithm is used to find the eigenvalue and rank-one residue matrix for each mode contributing at the peak. These operations are described in the following sections. Each eigenvalue and corresponding rank-one residue matrix is then used to construct an FRF model using eq. (2), which is subtracted from the FRF data. After removing the fit mode(s), the data within the frequency interval under consideration is zeroed to avoid the possibility of returning to this location to look for additional modes, as discussed in [15]. Removal of the contributions of the mode(s) contributing to the peak under consideration brings the next highest peak in the composite FRF into dominance. This peak is then searched for a mode or modes using the same procedure. The process continues until the composite FRF shows no coherent peaks suggestive of the presence of additional modes. Presently, this determination is made visually, as illustrated by the examples in subsequent sections. The mode isolation phase, in which the modes identified in the subtraction phase are iteratively defined, begins at this juncture.

2.1.1 Determination of the Number of Participatory Modes

In principle, visual comparison of each residual FRFs with the version synthesized from the modal parameters returned by the SDOF algorithm should reveal whether an SDOF fit represents the experimental data accurately. However, because FRFs from many input-output point combinations are available, assessing the quality of fit in each individual FRF can be tedious. It is more convenient to compare condensed data sets for the reconstructed FRF and the residual FRF of the mode in question. Such a comparison can be performed using the composite FRF in eq. (7), though multiple modes are often more easily identified on a Nyquist plot. One reason for this is that both close modes and noise can be manifested as peaks in a magnitude FRF. On a Nyquist plot close modes are more easily distinguished from noise features, as modes tend to look like circles or arcs while noise tends to show an irregular shape. However, there does not seem to be a standard definition of a composite FRF that retains phase

information. The composites formed by eq. (7) can not be used to create a Nyquist plot because they contain no phase information, while simple addition of FRFs can lead to cancellation of some modes' contributions, depending on their spatial phase. For example, adding FRFs for a symmetric structure would tend to reinforce symmetric modes while annihilating antisymmetric modes. For this reason a Nyquist composite FRF was defined in [6] as a weighted sum using the elements of the identified residue vector $\{(A_{\text{fit}})_r\}$ as weights. Use of the residue vector for mode r tends to reinforce mode r in the sum. The Nyquist composite FRF data $(H_{\text{cn}})_r(\omega)$ defined in [6] can found for a MIMO data set as follows

$$\begin{aligned}(H_{\text{cn}})_r(\omega) &= tr\left([(A_{\text{fit}})_r]^H * [H(\omega)]_{N_o \times N_i}\right) \\ &= \sum_{k=1}^{N_i} [(A_{\text{fit}})_r](:,k)^H * [H(\omega)](:,k)\end{aligned} \tag{9}$$

where $tr()$ is trace operator, $[(A_{\text{fit}})_r]$ is the current estimate of the residue matrix for the mode in focus and $[H(\omega)]$ is FRF data to be condensed. The notation $[X](:,k)$ signifies the kth column of matrix $[X]$. The data $(H_{\text{cn}})_r(\omega)$ can be plotted in the complex plane, resulting in what has been called a 'Nyquist composite plot.' Typical Nyquist composite plots may be found in the right panes of Figure 4 for an example that will be explored later.

In each subtraction step, the residual FRF is first compared with a reconstructed FRF found using the single set of modal parameters returned by the common-denominator, SDOF algorithm. In doing so, it is important to recognize that even when only a single mode is active at a particular peak, the residue matrix returned by the common-denominator algorithm $[A_{\text{fit}}]$ may have a rank greater than one, and thus not represent a true modal model (see eq. (2).) In order to obtain a consistent, SDOF, modal model, the singular value decomposition (SVD) of the fit residue matrix is formed,

$$[A_{\text{fit}}] = [U][S][V]^T \tag{10}$$

and the rank-one residue matrix is then found as

$$[A_{\text{fit,R1}}] = \{U_1\} S_1 \{V_1\}^T \tag{11}$$

where $\{U_1\}$ and $\{V_1\}$ denote the first left and right singular vectors respectively and S_1 denotes the first singular value. An FRF matrix for this mode is constructed using $[A_{\text{fit,R1}}]$, and visually compared to the residual FRF data on composite magnitude and Nyquist plots. Poor agreement between the FRFs reconstructed using $[A_{\text{fit,R1}}]$ and the residual FRFs usually indicates either that the peak is due to the presence of noise, or that more than one mode is present in the frequency interval. One method for discerning these scenarios involves consideration of the FRFs reconstructed using the full rank residue matrix $[A_{\text{fit}}]$. When the residual FRFs do not contain a mode, the FRFs reconstructed using a full rank residue matrix tend to compare with the data as poorly as the FRFs reconstructed using a rank-one residue matrix. However, when multiple modes are active in the frequency interval the FRFs reconstructed using a full rank residue matrix generally show better agreement with the data than the FRFs reconstructed using a rank-one residue matrix. In such a case, a higher order fit is sought.

Application of a multi-mode fit to the frequency interval under consideration requires knowledge of the number of modes active in the interval. A conventional approach for determining the number of modes active in a frequency region is to use a mode indicator function, which graphically displays the effective rank of the FRF matrix at each frequency [20]. In the present situation there is a convenient alternative. Application of a common-denominator fitting algorithm to the peak data results in a mode whose residue matrix has a rank comparable to that of the FRF matrix over the region spanned by the peak data. To explain this phenomenon, note that $[A_{\text{fit}}]$ is a valid residue matrix for a system having a single eigenvalue with multiplicity N_i. When a system has close eigenvalues, the common-denominator algorithm approximates the response near the peak with that of a system having a single eigenvalue, whose multiplicity equals the number of close eigenvalues. The rank of the common-denominator residue matrix $[A_{\text{fit}}]$ is revealed by the singular values contained in the diagonal matrix $[S]$ found previously via singular value decomposition. The ratio of each singular value to the first gives a measure of its significance. Mathematically, the singular value ratio for the kth singular value is given by

$$SR_k = S_k/S_1. \tag{12}$$

The number of singular value ratios near unity indicates the effective rank of the residue matrix, and hence the number of modes that are active in the frequency band of interest. As a rule of thumb, singular value ratios above

0.25 typically indicate the presence of additional modes. Using this approach, it is possible to detect the existence of close modes in the peak data, even when only a single peak is visible.

When multiple modes are detected, an MDOF fit of the order indicated by the singular values is applied to the data using the MIMO, MDOF algorithm described below. If all singular values are significant, the user may choose to apply fits of increasing order and compare the resulting reconstructed FRFs with the residual FRFs in order to determine if additional modes are present.

It is useful to have a quantitative metric expressing how well the reconstructed FRFs agree with the residual FRFs near the peak in focus. Towards this end, an FRF Reduction Factor RF is defined according to

$$RF = \frac{\max\left(composite\left(\left[H\left(\omega\right)\right]\right)\right)}{\max\left(composite\left(\left[H\left(\omega\right)\right] - \left[\left(H_{\text{fit}}\right)_k\left(\omega\right)\right]\right)\right)}. \tag{13}$$

where the FRF matrix reconstructed from the mode or modes identified at the kth peak (or kth step of the subtraction stage) is designated $\left[\left(H_{\text{fit}}\right)_k\left(\omega\right)\right]$. This metric is constructed from data in a frequency band that is twice as wide as that used in the fit in order to quantify how well the fit can be extrapolated. Values greater than unity indicate that the FRFs would be reduced by subtracting the contribution of the mode under consideration. Typically, values greater than 3 indicate a good fit.

2.2 Mode Isolation Stage

Once all of the modes of the system have been approximated, the estimate for each mode is refined through an iterative procedure to account for the possibility of overlapping contributions from other modes. At this stage the algorithm proceeds through the groups of modes in the same sequence in which they were identified. Previous versions of AMI isolated individual modes in each step. In the hybrid approach either single modes or groups of closely spaced modes found simultaneously during the subtraction stage are "isolated" as follows. First, the contributions of all modes except for those in focus are subtracted from the FRFs. A modal fit to the resulting residual FRF is then performed using either the common-denominator, SDOF algorithm if a single mode is being isolated, or the MIMO, MDOF algorithm if a group of closely spaced modes is being isolated. The model is then updated with the newly identified modal parameters and the algorithm proceeds to the next group. A cycle through all identified groups constitutes one iteration. Computations cease when the largest change in any eigenvalue or any element of any residue matrix falls below 0.001%. Typically only a few iterations are required.

2.3 MIMO, MDOF Fitting Algorithm

Several MIMO, frequency domain algorithms have been presented in the literature. Many are common-denominator algorithms, which work well when identifying distinct modes, but might miss very closely spaced modes or yield a poor fit for close modes after their residue matrices are reduced to rank-one, see [21], [22], and [23]. A few algorithms directly identify a consistent modal model, i.e. one that has rank-one residue matrices. Such a result is obtained when a right matrix fraction polynomial model is fit to the data [21], [23], though such a model requires that the number of modes estimated be an integer multiple of the number of inputs. Another alternative, the Frequency Domain Direct System Parameter Identification (FDDSPI) algorithm (also called Poly-Reference Frequency Domain (PRFD) in [24]) has the same limitation. The frequency domain subspace algorithm (SSI-FD) presented by Van Overschee and De Moor in [25] offers an attractive alternative, in which the number of modes estimated is not required to be a multiple of either the number of inputs or outputs. Van Overschee and De Moor present two subspace algorithms in [25], a "simple" algorithm that suffers from ill-conditioning in the data matrices for high model order, and an algorithm in which the ill-conditioning is reduced using Forsythe orthogonal polynomials. Because AMI only needs to simultaneously identify a few modes, the simple algorithm was implemented. This simple SSI-FD algorithm was found to be surprisingly fast when fitting a small amount of data with a low order fit, and ill conditioning was not encountered.

3 Application I: Cantilevered Frame System:

This first test problem serves to demonstrate the effect of varying noise levels, weakly excited and localized modes, and close modes. This test problem has been used previously to assess earlier implementations of AMI [5], [6], [11] and [12]. The problem was described in detail in [5], where the SISO version of AMI was used with the identical data set. The problem consists of two orthogonal cantilevered beams, welded at their free ends, as depicted in Figure 1.

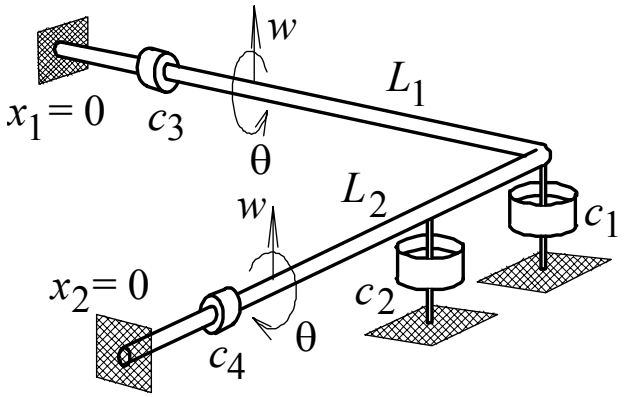

Figure 1: Schematic of Cantilevered Frame System.

Mode	ω_r	$\zeta_r * 100$
1	68.008	0.9653
2	265.91	0.06169
3	386.32	0.12491
4	829.45	0.03220
5	1033.8	0.07676
6	1697.0	0.03599
7	1937.9	0.16103
8	2479.7	0.75799
9	2511.0	0.72183
10	2995.7	0.17847
11	3380.0	0.15417

Table 1: Eigenvalues for First 11 Modes

The system was modeled using the Ritz method as described in [19]. The twenty-one lowest eigenvalues and associated mode functions obtained from a Ritz series analysis of the system were used to construct the impulse response resulting from excitation at one meter from the clamped support of the first beam, and then a second impulse response resulting from excitation at one meter from the clamped support of the second beam. ($P_1 = 1$, $P_2 = 9$, see eqs. (2) and (14).) The displacement and rotation as a function of time at seven points on the structure due to an impulsive force were obtained by synthesizing the Ritz series. The resulting response vector $\{y\,(t)\}$ contains both displacements and rotations at locations one meter apart,

$$\{y\,(t)\} = [w_1\ w_2\ w_3\ w_4\ \theta_1\ \theta_2\ \theta_3\ \theta_4\ w_5\ w_6\ w_7\ \theta_5\ \theta_6\ \theta_7\ \theta_8]^{\mathrm{T}} \tag{14}$$

where the first eight elements are measured on the first beam and the last seven elements are measured on the second beam.

The analytical responses were sampled, and then noise contaminated by adding normally distributed white noise with zero mean and standard deviation scaled to 1% of the maximum of each impulse response. The noise contaminated impulse responses were then transformed to FRFs via a Fast Fourier Transform. The sample rate was chosen to satisfy the Nyquist criterion. Originally, 2^{16} samples were created resulting in negligible leakage in the FRFs. It was found that accurate results could be obtained by processing only 2^{13} samples, even though significant leakage was present in the FRFs (see [6].) Truncating the data set reduces the effect of noise on the quickly-decaying, high frequency modes, so that they are identified more accurately from the shorter data set. While the low-frequency modes suffer from leakage, the decrease in accuracy for these modes is small. Another reason for truncating the data set is that the modal parameters found by applying MIMO-AMI will be compared to those found by the stochastic subspace identification algorithm (SSI). Use of the shortened data set for AMI allows for a direct comparison with the SSI algorithm, which could not process the full 2^{16} sample data set due to the limited memory of the computer running the algorithm. The identification that follows was focused on a band of frequencies containing only the lowest 11 modes. The analytical natural frequencies and damping ratios for these modes are shown in Table 1.

The high frequency modes (8-11) are fairly well represented in the rotation data, as typified by Figure 2, whereas their peaks are much smaller in the displacement FRFs, of which Figure 3 is typical. A single peak is evident in the vicinity of modes 8 and 9 in Figure 2, but the peak could be mistaken for the shoulder of an anti-resonance in Figure 3. Inspection of the mode functions for modes 8 and 9 presented in [5] revealed that these modes are localized in their displacement portions to the second and first spans of the frame respectively. Thus, a single excitation applied to either span does not adequately excite both modes 8 and 9.

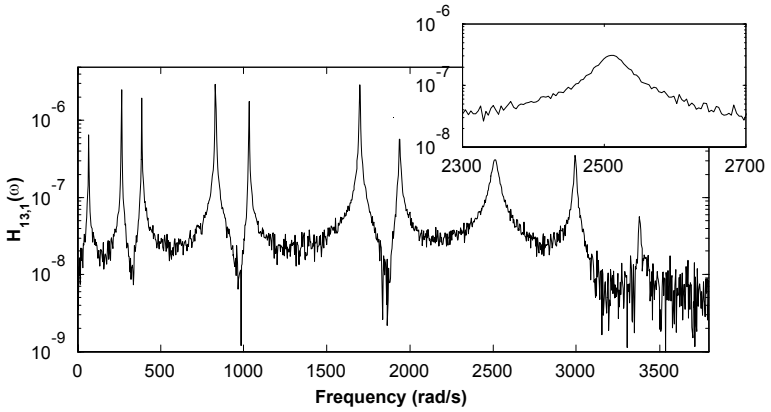

Figure 2: Noisy rotation FRF at 2 m from clamped support on beam 2.

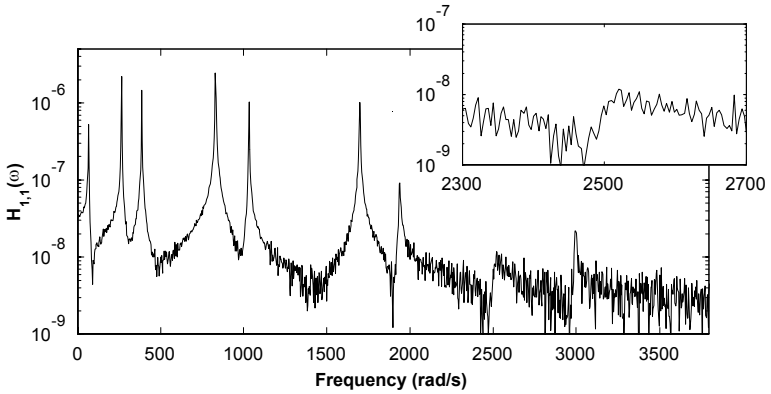

Figure 3: Noisy displacement FRF at 1 m from clamped support on beam 1.

3.1 MIMO-AMI Results

After each mode is fit in the subtraction phase, the reduction factor RF is found according to eq. (13), in order to assess how well the FRFs reconstructed from the modal parameters identified in that subtraction step compare to the residual FRFs. Modes 1-7 yielded reduction factors ranging from 45 to 385, indicating a very good fit to the data. For each of these modes, the second singular value ratio SR of the residue matrix was small, indicating that the residue matrix obtained from the SDOF fit was effectively rank-one.

The left panes in Figure 4 display the composite of the residual FRFs for subtraction steps 8 to 11. Composites of the FRFs constructed from the modal parameters identified in each subtraction step are also shown. On the right, composite Nyquist plots of the residual data and fit are shown. Mode 10 was identified in the eighth step with $RF = 5.9$ and $SR_2 = 0.03$. In the ninth step, an SDOF fit to the peak in which analytical modes 8 and 9 are situated resulted in $RF = 1.2$ and $SR_2 = 0.78$. Use of the full rank residue when synthesizing the model resulted in a larger reduction factor. These indicators suggest that an additional mode is present at the peak. Two singular value ratios were found to be greater than 0.25, so a 2-DOF fit was attempted. Application of a 2-DOF fit using the SSI-FD algorithm resulted in $RF = 3.6$ for an FRF constructed from the two modes that resulted.

Composite Nyquist plots are also shown for this subtraction step. The definition of the composite Nyquist data uses the residue matrix for a specific mode. Each mode identified at subtraction step nine has a distinct residue matrix, so a composite Nyquist plot was created for each. These are shown in the right panel in Figure 4 (solid lines,) where they are compared to a residual FRF of the data, formed by subtracting from the measured FRF the contribution of all identifed modes except for the mode in focus. Both the reconstructed and residual FRFs were condensed using the residue matrix for the mode in focus in eq. (9). This resulted in a reconstructed and residual Nyquist composite FRF for each mode. The Nyquist composites for mode 10 were multiplied by -1 and plotted in gray to aid in distinguishing them from those for mode 9. The composite magnitude plot reveals that the data has been reduced to noise in the vicinity of these modes, so use of an even higher-order fit is not warranted. Subtraction step ten led to identification of another mode, with $RF = 3.8$ and $SR_2 = 0.03$. As step 11 is initialized, the residual FRF obtained by subtracting the contribution of the modes identified in steps one through ten appears in the last pane of Figure 4. The data has been reduced to noise. Attempts to extract additional modes from this data result in modes with reduction factors below 1.0.

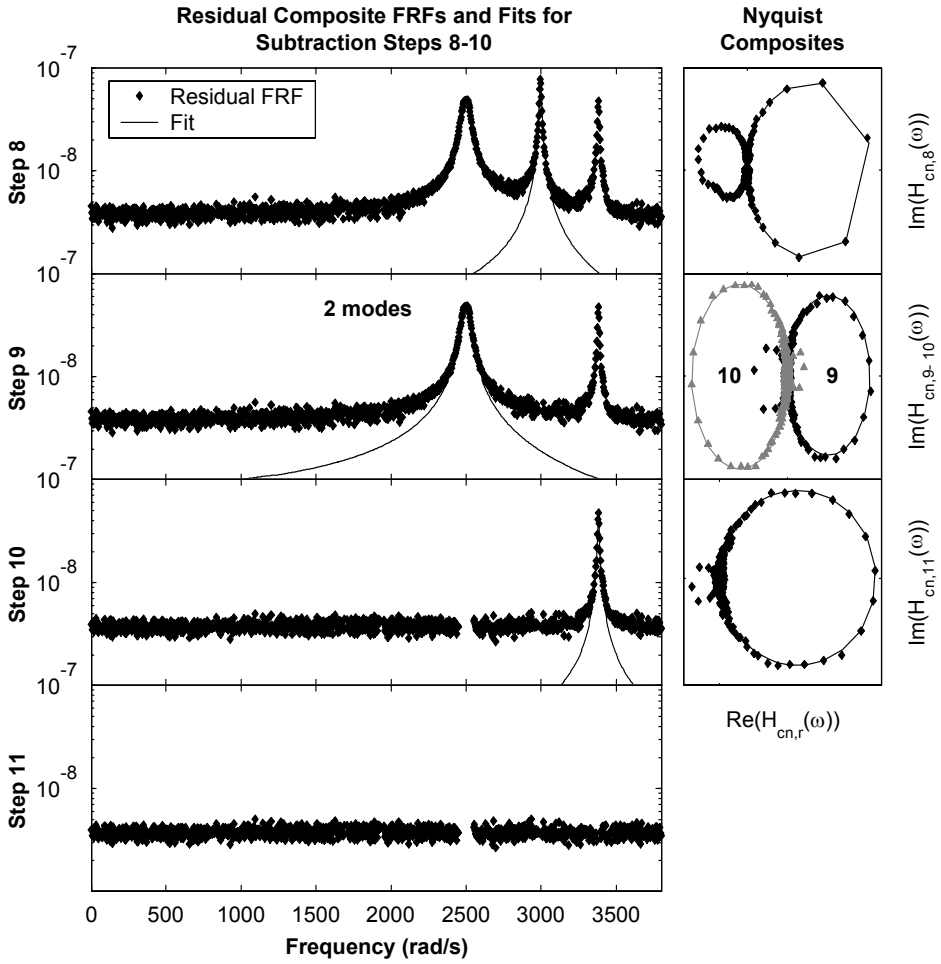

Figure 4: AMI subtraction steps 8-11 for short-record frame data. Left: composite residual FRFs (.) and composite fits (-). Right: Composite Nyquist plots of residual data (.) and fit (-). Each composite Nyquist plot was created using the residue matrix for the mode in focus.

AMI next proceeds to the mode isolation stage. After three iterations in mode isolation the maximum change in either eigenvalues or residues was less than 0.001%. The eigenvalues and mode shapes found by AMI compared very well with the analytical ones.

A Monte Carlo simulation was performed in order to obtain a characterization of the results that is independent of the random noise sequence applied to the impulse response. Towards this end, thirty normally distributed,

zero-mean noise profiles, scaled to have a standard deviation equal to 1% of the maximum impulse response, were created and stored to disk so that the same noise profile could be used for both AMI and SSI. The errors in the natural frequencies and damping ratios found by AMI for all thirty trials are presented in Figure 5. The distribution of these errors illustrates the bias and scatter of the algorithms. The scatter is characterized by the width of the distributions, higher scatter indicating that larger errors are possible for any given noise profile. The center of the distributions defines the bias. A bias different from zero represents the average error obtained when the experiment is repeated a number of times. The bias errors in Figure 5 are generally smaller than the trial to trial scatter. Comparison of the results of MIMO-AMI with those presented in [6] for SIMO-AMI show that the MIMO algorithm results in much more accurate results for the parameters of mode 8. This is due primarily to the fact that the additional input excites mode 8 much more effectively than the original input applied in the SIMO analysis.

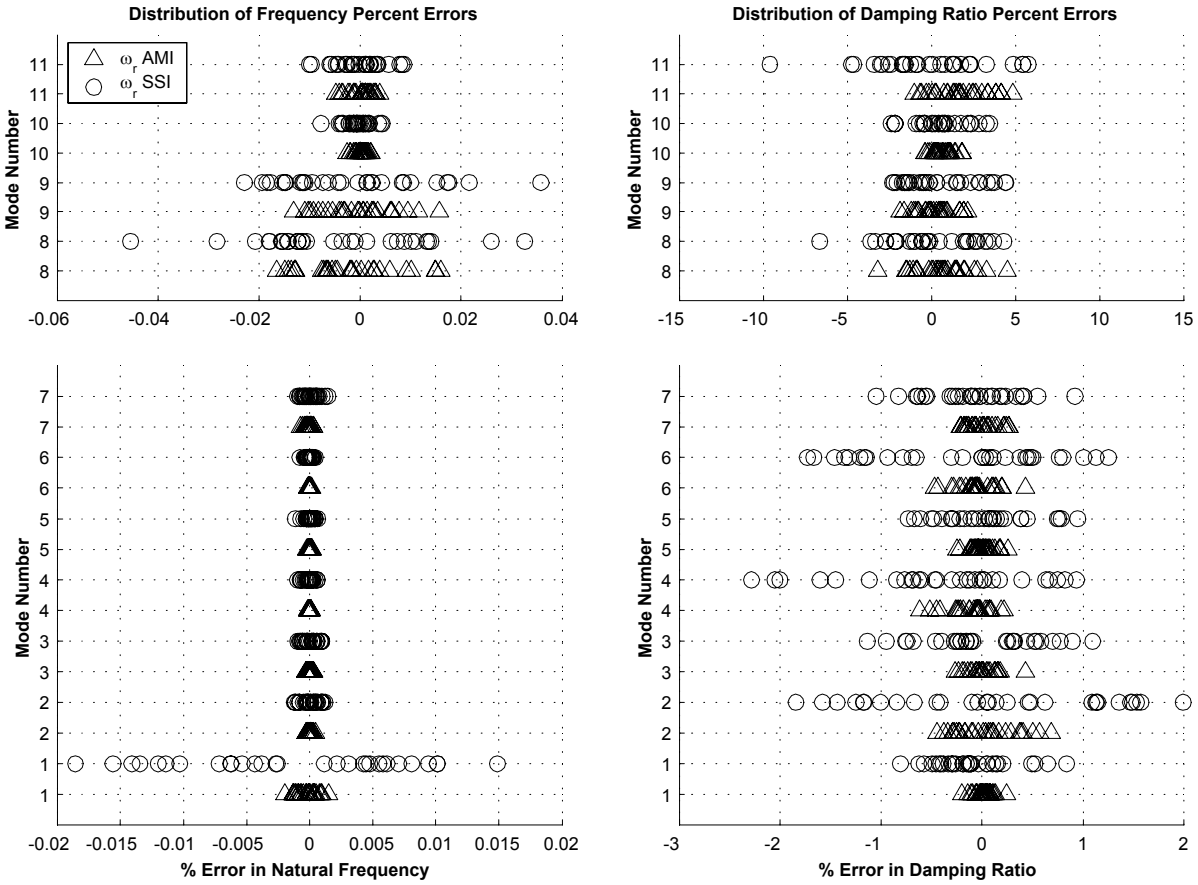

Figure 5: Result of Monte Carlo Simulation for Frame structure. Errors in Natural Frequencies and Damping Ratios for thirty trials of AMI and SSI.

3.2 SSI Results

The Stochastic Subspace Identification algorithm [26] was also used to process the noise contaminated analytical data for the L-shaped frame. The specific stochastic algorithm used was included in the software tools supplied with [26] implemented in the function "subid.m." For more detail, see [26] or [27]. While memory requirements and processing time can be considerable for the SSI algorithm, it tends to yield very clear stabilization diagrams and accurate results. It has been used in comparisons with previous versions of AMI in [3] and [6]. In those comparisons it was noted that clear stabilization diagrams and accurate results were not obtained unless enough block rows were used in forming the Hankel Matrices. Those studies revealed that very clear stabilization diagrams were obtained when 16 or more block rows were used, while 32 block rows were needed to accurately identify the pair of close modes (modes 8 and 9.) Use of 64 block rows resulted in substantial improvements in the eigenvalues of modes 1, 2 and 8 when compared to the results for 32 block rows. Little change was seen in the bias and scatter of the eigenvalues

for the other modes. Because of memory limitations, no more than 64 block-rows could be used.

When the response of a structure at a large number of points is measured, it is common to sucessively collect a small subset of the measurements to minimize the number of sensors needed. Each patch of measurements is typically procesed independently when the SSI algorithm is applied to such a data set. The eigenvalues obtained from each patch are then averaged to obtain a global set. For example, this approach was used in [28]. In accord with this practice, SSI was applied to the set of all responses for each of the drive points separately. The application of SSI to data for the first drive point was presented in [3] and [6], in which sample stabilization diagrams were presented. The second drive point gave similar results. In each case, SSI used a model order of 42 (21 modes) with 64 block-rows in data Hankel Matrix. Use of larger model orders did not result in a noticeable improvement. For this model order SSI identified a small number of spurious modes in the frequency band of interest. As shown in [3], the spurious poles were easily distinguished because they had substantially higher damping ratios than the true poles.

Because the data from each drive point was processed independently, SSI gave two estimates for each eigenvalue for each trial in the Monte-Carlo experiment. A consequence of the localized nature of mode vectors 8 and 9 is that they were excited much more effectively, and thus were identified much more accurately, in the data sets for the second and first drive points, respectively. Standard practice would be to average the eigenvalues from each data-set, resulting in averaged eigenvalues for modes 8 and 9 that were less accurate than the estimates from a well chosen drive point. An experienced analyst might take note of the weak excitation of modes 8 and 9 in the first and second drive points, respectively, and choose to discard the estimates of each eigenvalue from the data set in which it was weakly excited. Correspondingly, in the results presented herein, SSI's eigenvalues from each drive point were averaged for all modes except 8 and 9. For modes 8 and 9 the eigenvalues from the drive point in which the mode was most strongly excited were retained. The resulting errors in the natural frequencies and damping ratios in each trial are plotted in Figure 5. It should be noted that simply averaging the results from each drive point for all of the modes resulted in 2-3 times greater scatter in the natural frequencies and damping ratios for modes 8 and 9 than that shown in Figure 5.

Overall, the results of the SSI algorithm compare quite well with those of the AMI algorithm for many of the modes. AMI results in considerably less scatter in the damping ratios for modes 1-7. AMI also gives much more accurate results for the natural frequency of mode 1 and somewhat more accurate results for the natural frequencies of modes 8-11. The results for most of the other modes are comparable. The AMI algorithm required significantly less computation time than the SSI algorithm, and did not require the use of a stabilization diagram.

4 Application II: Simply-Supported Plate:

The closest modes in the frequency band processed for the frame problem, modes 8 and 9, were separated by 85% of their mean half-power bandwidth and were localized in their displacement patterns. Systems that have globally active modes with close natural frequencies present a different challenge. This section describes an application of MIMO-AMI to noise-contaminated synthetic FRF data for a simply-supported rectangular plate. The analytical solution for a simply-supported Euler plate yields the natural frequencies and mode functions for the plate. Each mode was assigned a modal damping ratio of 0.02. The aspect ratio of the plate, a/b, was chosen to be 1.001, resulting in three pairs of very close modes in the frequency band of interest whose natural frequencies were separated by 3%, 4% and 2% of their average half-power bandwidths. A nine by nine grid of uniformly distributed measurement points was assigned to the face of the plate. The analytical modal parameters were used to derive the velocity impulse response of the plate for excitation at three different locations. (The velocity response was used to mimic an experiment in which a laser pulse is used to excite the plate and a laser doppler vibrometer is used to measure the plate's vibration.) For a plate having side lengths a and b in the x and y directions respectively, the drive points coordinates $[x, y]$ were, $[0.2a, 0.2b]$, $[0.3a, 0.7b]$ and $[0.6a, 0.7b]$. These drive points were chosen to ensure excitation of the first eight modes of the structure. Frequency was non-dimensionalized such that $\omega_{\rm nd} = \omega a^2\sqrt{\rho h/D}$, where D is the flexural rigidity of the plate. The analytical mode functions are $\sin(n\pi x/a)\sin(m\pi y/b)$ were n and m are integers. The modes for indices n and $m \leq 5$ were used to generate the impulse response of the plate, resulting in 25 modes being included in the impulse response. Normally distributed Gaussian noise, scaled to have a standard deviation equal to 2% of the maximum in each response point, was added to the velocity impulse responses. The sampling rate and time window were chosen to avoid aliasing and minimize leakage. After transferring the impulse response to the frequency domain, the analysis focused on a band of frequencies in which the lowest 8 modes of the plate were active. Figure 6 shows the response measured at the third drive point with excitation applied at the first, which typifies all FRFs. Figure 7 shows a composite FRF formed from all 243 FRFs.

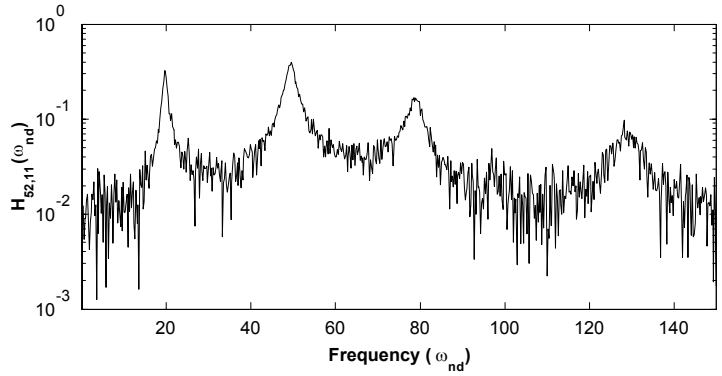

Figure 6: Simply supported plate data. FRF for the response at the third drive point with excitation applied at the first drive point.

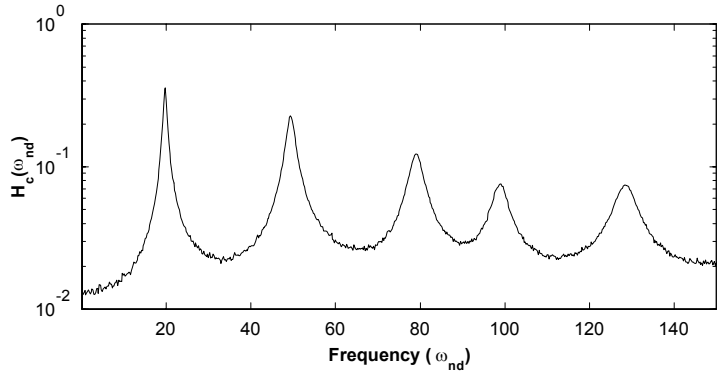

Figure 7: Simply supported plate Data. Composite FRF for simply supported plate data.

4.1 pLSCF Results

Because of the large number of output points used in the response, the memory and processing time required to accurately process this data set using SSI exceeded available resource. For this reason, the FRFs were processed by the polyreference Least Squares Complex Frequency Domain (pLSCF) algorithm (see [22], [23] and [29],) which is also known as the Polymax® algorithm in the LMS software package. The algorithm used here was written in Matlab by the authors based on the information presented in the cited references. The pLSCF algorithm was tested on noise-free FRFs for the plate response and found to give very accurate results, (i.e. errors on the order of 10^{-7} percent for the natural frequencies and 10^{-5} percent for damping ratios.) The pLSCF algorithm is a very fast algorithm capable of quickly processing data from a large number of sensors. It has received considerable attention because of its speed and because it tends to yield unambiguous stabilization diagrams. In [22] Van Der Auweraer et al presented an FFT technique to speed up creation of the normal equations, but that procedure was not used here. Doing so would might reduce the processing time of the algorithm, but should not affect the final results.

A stabilization diagram created from the eigenvalues identified by pLSCF is shown in Figure 8. No unstable modes (i.e. $\mathrm{Re}\{\lambda\} > 0$) were returned by the pLSCF algorithm. Several overdamped modes were identified; they are not shown in Figure 8. A number of computational modes are identified by the algorithm, especially as the model order becomes very large. Some of these spurious modes are distinguishable from the computational modes because they have much larger damping ratios. This is illustrated in Figure 8 by marking the modes with damping ratios less than 5% with circles and those with damping ratios greater than 5% with crosses. This clarifies the stabilization diagram considerably. For convenience, dashed vertical lines are shown at the natural frequencies of the true modes of the system. The first four modes of the system, corresponding to the three left-most peaks in Figure 8 are identified reliably for model orders greater than 21. A higher model order is needed before the higher frequency modes stabilize, and a considerable number of spurious modes are identified before all of these modes are consistently identified. A

magnified view would show pairs of close modes near $\omega_{\mathrm{nd}} = 50, 100$ and 130. As an example, a view focusing on the modes near $\omega_{\mathrm{nd}} = 100$ is shown in Figure 9. At most model orders only two stable, lightly damped modes are found, indicating that the pLSCF algorithm has correctly determined the mode multiplicity in this frequency band. The scatter in the natural frequencies from one model order to the next is considerably larger than their separation. The scatter relative to the modal separation for the modes near $\omega_{\mathrm{nd}} = 130$ was worse than this, whereas that of the modes near $\omega_{\mathrm{nd}} = 50$ was less than their frequency separation. Clearly the accuracy obtained when using the pLSCF algorithm depends strongly on the model order, although Figure 9 suggests that the most accurate results are found for model orders greater than 50. The range of natural frequencies and damping ratios found by the pLSCF algorithm for model orders ranging from 51 to 90 is shown in Table 2.

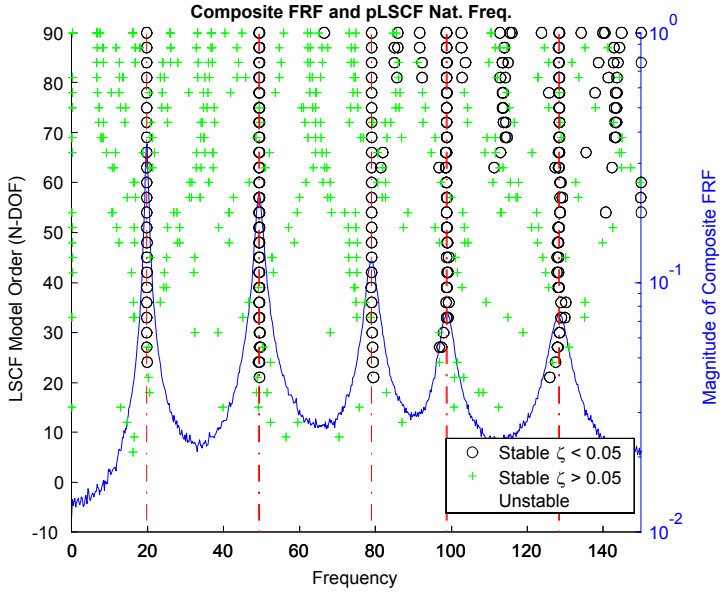

Figure 8: Simply supported plate data. Stabilization diagram for LSCF algorithm.

4.2 Hybrid, MIMO-AMI Results

AMI was also applied to the plate data. As for the frame system, a peak selection factor of $\alpha = 0.5$ was used. The subtraction process was automated for this analysis by attempting an MDOF fit at each peak for which the full-rank residue resulted in a reduction factor greater than 3.0 and the rank-one residue resulted in a reduction factor less than 3.0. If these conditions were met, the number of modes fit at the peak was given by the number of singular value ratios greater than 0.25. All modes or sets of modes with reduction factors greater than 3.0 were retained. Subtraction halted when the full-rank residue matrix yielded a reduction factor less than 3.0. This approach resulted in five subtraction steps being performed, each of which obliterated one of the peaks in the composite FRF. At each peak containing a pair of close modes, the second singular value ratio was greater than 0.5, while the third singular value ratio was below 0.1, suggesting that a two mode fit was indeed appropriate. The subtraction phase resulted in initial estimates of the properties of eight modes, which is the number contained in the frequency band that was processed. Subtraction of these eight modes from the data left no coherent peaks. Five iterations in mode isolation phase were performed. In the last iteration the maximum change in either eigenvalues or residues was less than 0.001%. After mode isolation, the reconstructed FRFs for each individual mode, when viewed on a composite Nyquist plot, were found to agree more closely with the data than before mode isolation. A similar comparison using a composite magnitude plot showed no noticeable change. Figure 10 shows magnitude composite plots of the noisy FRFs, AMI's reconstructed FRFs after the mode isolation phase, and a magnitude composite of the difference between the two. Table 2 compares the analytical natural frequencies and damping ratios with those found by AMI. The average errors in the natural frequencies and damping ratios found by AMI were respectively 0.006 % and 2 %.

Figures 11 through 15 show contour plots of the imaginary parts of the mode vectors found by AMI for each mode. Because a modal damping model was used, the real parts of each mode vector should be zero. The norm of the real parts of the mode vectors identified by AMI divided by the norm of their imaginary parts gives a measure of the

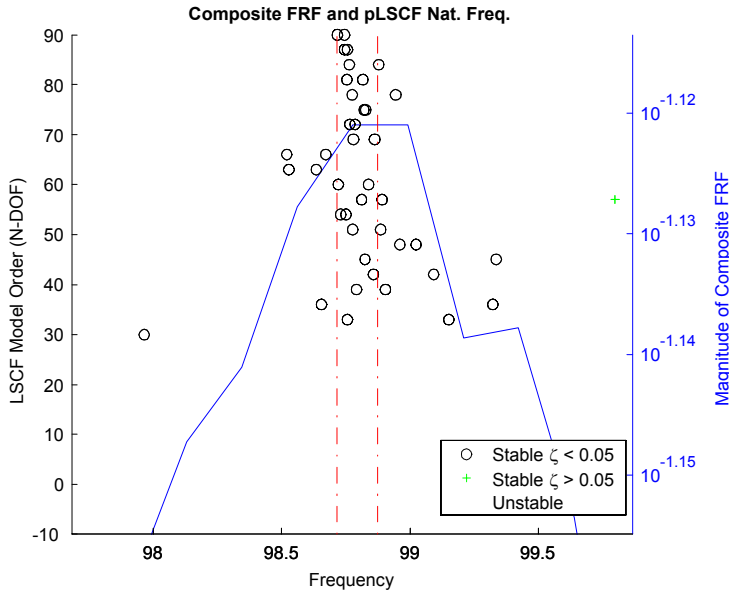

Figure 9: Simply supported plate data. Zoom view of stabilization diagram showing two close modes. The dashed (red) vertical lines show the true natural frequencies.

	Actual		**MIMO-AMI**		**pLSCF***	
Mode	$\boldsymbol{\omega}_r$	ζ_r	$\boldsymbol{\omega}_r$	ζ_r	$\boldsymbol{\omega}_r$	ζ_r
1	19.759	0.02	19.758	0.0199	19.749 - 19.763	0.0208 - 0.0221
2	49.3678	0.02	49.369	0.0202	49.357 - 49.383	0.0211 - 0.0234
3	49.427	0.02	49.421	0.0200	49.421 - 49.438	0.0207 - 0.0220
4	79.0358	0.02	79.029	0.0194	79.000 - 79.054	0.0208 - 0.0220
5	98.716	0.02	98.705	0.0191	98.521 - 98.824	0.0217 - 0.0263
6	98.874	0.02	98.855	0.0194	98.745 - 98.944	0.0219 - 0.0291
7	128.384	0.02	128.366	0.0195	128.13 - 128.67	0.0213 - 0.0289
8	128.483	0.02	128.508	0.0196	128.38 - 129.29	0.0206 - 0.0294

Table 2: Actual, AMI, and pLSCF Eigenvalues for First 8 Modes of Simply Supported Plate. *Range of values for pLSCF show the variation in each parameter for model orders from 51 to 90.

relative size of the real parts. For the distinct modes 1 and 3, the ratios were on the order of 1e-4, while the pairs of close modes gave ratios ranging from 0.01 to 0.13. The mode shapes shown in Figures 11 through 15 compare very well with the analytical ones, the analytical shapes being made up of various numbers of half sines in the x and y directions. Some distortions are visible, most notably in Figure 12 where the nodal lines for modes 2 and 3 are rotated slightly.

5 Conclusions

A MIMO implementation of the Algorithm of Mode Isolation was presented and applied to two prototypical systems. The results of the MIMO-AMI algorithm were compared to those of two conventional algorithms, the Stochastic Subspace Identification Algorithm (SSI) and the poly-reference Least Squares Complex Frequency domain (pLSCF) algorithm. In both test problems the true modes extracted by these benchmark methods were located using stabilization diagrams. When applied to data for the cantilevered frame system, the SSI algorithm gave good accuracy so long as enough block rows were used in the Hankel matrix. As noted in [6], clear stabilization diagrams were obtained from SSI when 16 or more block rows were used, though 32 block rows were needed to accurately distinguish modes 8 and 9, whose natural frequencies differ by less than their average half power bandwidth. A Monte Carlo simulation revealed that increasing the number of block rows from 32 to 64 resulted in a significant decrease in the bias and scatter in the modal parameters for modes 1, 2 and 8. Because of computational constraints,

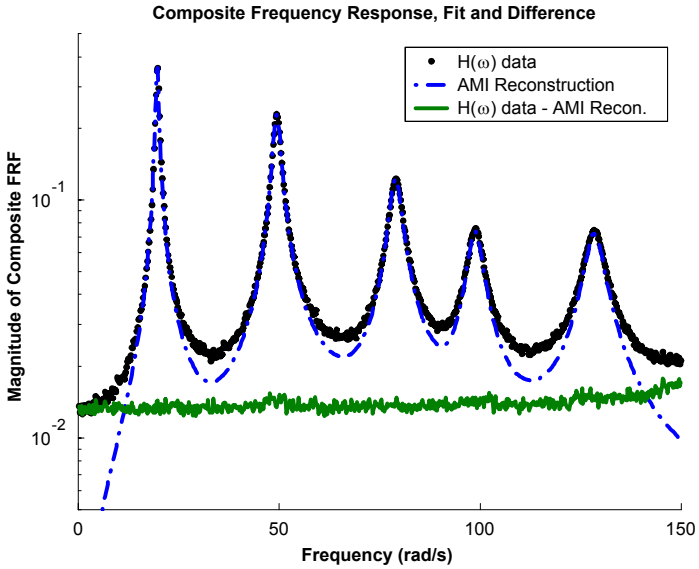

Figure 10: Magnitude composites of the noisy FRF data, AMI's reconstruction and the difference between the two.

no more than 64 block rows could be used in the SSI algorithm. The AMI algorithm showed less scatter in the identified natural frequencies and damping ratios, when compared to SSI applied using 64 block rows.

A second test problem involved a rectanguar plate whose aspect ratio was very close to unity. An aspect ratio of one was not used in order to avoid the ambiguity of multiple modes at the same natural frequency. In a separate analysis not presented here, AMI was applied to synthesized data for a plate with an aspect ratio of unity. AMI correctly identified the mode multiplicity at each peak for this data set, and the resulting mode vectors were recognizable as linear combinations of the products of sines, as expected for a simply supported square plate.

The rectangular plate problem illustrated the performance of the MIMO-AMI and pLSCF algorithms on a data set with a relatively large number of FRFs. The individual FRFs for the rectangular plate were quite noisy, and would have been difficult to process using a SISO algorithm. However, because of the large amount of redundant information available in the total set of FRFs, global processing resulted in accurate estimates of the modal parameters. The pLSCF algorithm was shown to quickly identify the modes of the structure and accurately identify the number of modes dominant at each peak, although the scatter in the natural frequencies that pLSCF identified was larger than the separation between the analytical natural frequencies. While such small differences might not be of interest in all applications, they could be important in demanding applications, such as damage detection or inverse problems. Furthermore, with the pLSCF algorithm there was no clear way of determining which model order resulted in the most accurate estimates of the modal parameters. Table 2 shows that relatively large errors were possible, depending on which model order was used. Because of the relatively high noise in the data, the iterative maximum-likelihood version of the pLSCF algorithm [30], an implementation of which was not available to the authors, might have been preferred in this application.

Two metrics, the Reduction Factor RF and the ratio SR of the singular values of the residue matrix, were introduced to assist in making decisions when AMI was applied to the data sets. These were used to determine the number of modes to be fit at each peak in the initial stage of AMI, in which modal contributions are subtracted from the data. Based on these metrics, the subtraction stage was performed automatically when AMI was applied to the plate data, though some intervention was required to process the FRFs for the frame system. The values used here in automating the subtraction process work well for extracting the dominant modes from data for a variety of systems, though additional research is needed before all operations can be automated for an arbitrary system. Nevertheless, the modal properties of both test systems were accurately identified using MIMO-AMI with little user interaction. There was no need for a stabilization diagram; the number of modes in the frequency band was identified as part of the algorithm's operation. Also, the AMI algorithm was able to globally process all available FRFs very quickly because it uses low order fits restricted to data near the resonant peaks.

Because MIMO-AMI employs an MDOF identification scheme when modes are close, there exist, at least theoretically,

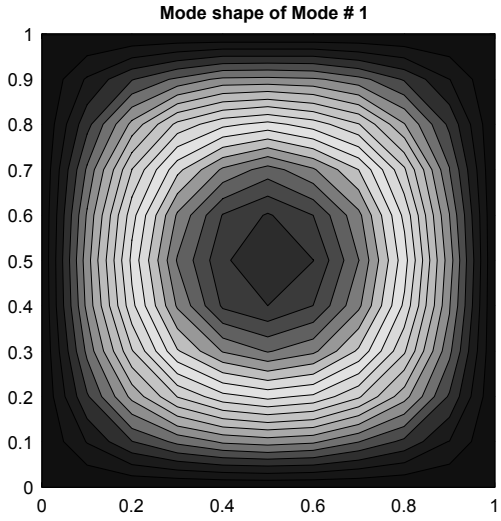

Figure 11: MIMO-AMI algorithm: Contour plot of the imaginary part of the first mode vector.

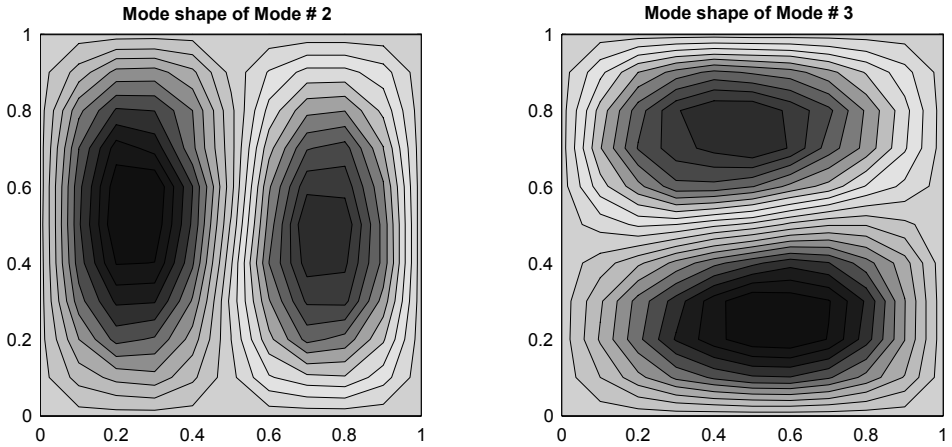

Figure 12: MIMO-AMI algorithm: Contour plot of the imaginary part of mode vectors two and three.

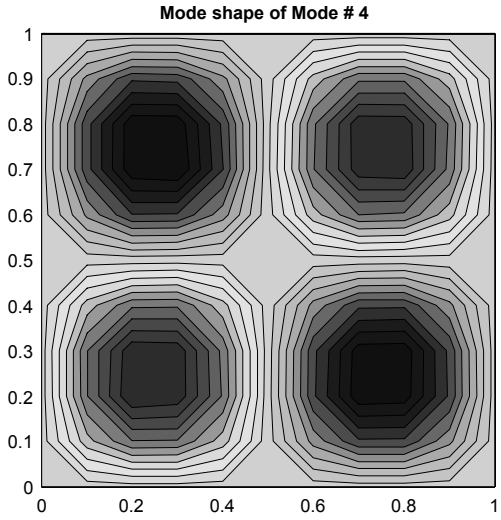

Figure 13: MIMO-AMI algorithm: Contour plot of the imaginary part of the fourth mode vector.

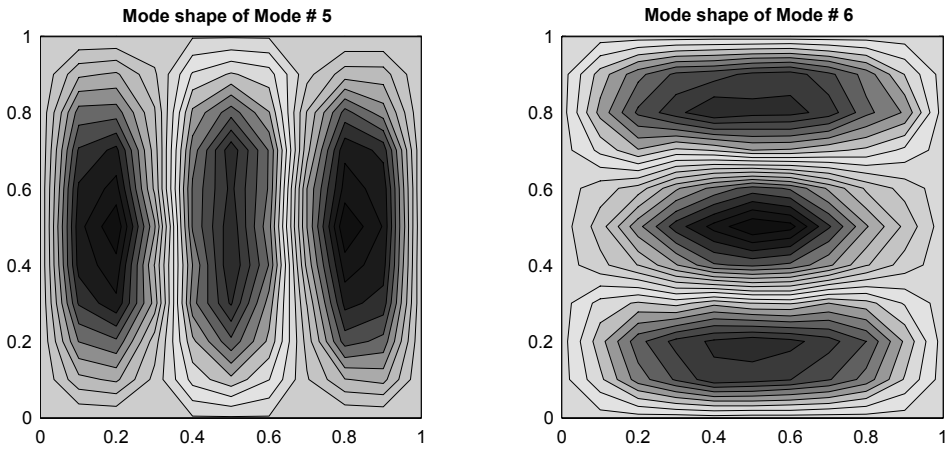

Figure 14: MIMO-AMI algorithm: Contour plot of the imaginary part of mode vectors five and six.

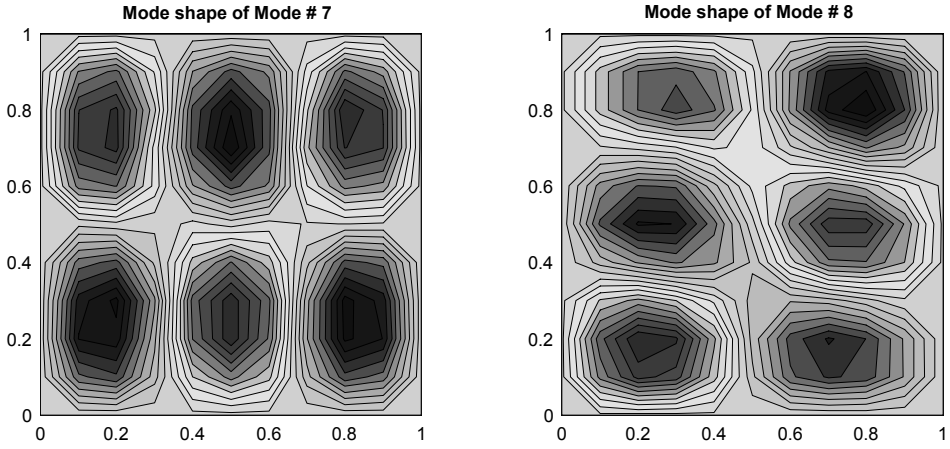

Figure 15: MIMO-AMI algorithm: Contour plot of the imaginary part of mode vectors seven and eight.

systems to which MIMO-AMI would offer no advantage over conventional methods. For example, suppose the separation between each natural frequency and its neighbors is less than 50% of the average half-power bandwidth. A composite FRF for such a system might show only one broad peak, so that the hybrid algorithm would be required to process the FRF data encompassing all of the modes of the system simultaneously. This is the typical MDOF approach. Such a situation often occurs in the very high frequency range of built-up systems, but that is not where EMA is usually performed. In the lower frequency regime only a few modes are likely to be clustered in a narrow frequency interval. In such cases the fact that AMI only processes peak FRF data significantly enhances its computational efficiency and its robustness in the presence of noise.

ACKNOWLEDGEMENT

This research was supported in part by a National Science Foundation, Graduate Research Fellowship.

References

[1] Herman Van Der Auweraer, Willem Leurs, Peter Mas, and Luc Hermans, "Modal parameter estimation from inconsistent data sets," in *18th International Modal Analysis Conference (IMAC-18)*, San Antonio, Texas, 2000, pp. 763–771.

[2] Scott W. Doebling, Kenneth F. Alvin, and Lee D. Peterson, "Limitations of state-space system identification algorithms for structures with high modal density," in *12th International Modal Analysis Conference (IMAC-12)*, Honolulu, Hawaii, 1994, pp. 633–640.

[3] Matthew S. Allen and Jerry H. Ginsberg, "SIMO extension of the algorithm of mode isolation," in *IMAC 22 - XXII International Modal Analysis Conference*, Dearborn, Michigan, 2004.
[4] Michael V. Drexel and Jerry H. Ginsberg, "Mode isolation: A new algorithm for modal parameter identification," *Journal of the Acoustical Society of America (JASA)*, vol. 110, no. 3, pp. 1371–1378, 2001.
[5] Matthew S. Allen and Jerry H. Ginsberg, "A linear least-squares version of the algorithm of mode isolation for identifying modal properties. part ii: Application and assessment," *Journal of the Acoustical Society of America (JASA)*, vol. 116, no. 2, pp. 608–615, 2004.
[6] Matthew S. Allen and Jerry H. Ginsberg, "A global, single-input-multi-output (SIMO) implementation of the algorithm of mode isolation and applications to analytical and experimental data," *Mechanical Systems and Signal Processing*, vol. Submitted, 2005.
[7] J. Kirshenboim, "Sim - modal identification by simultaneous mode fitting," Tech. Rep., Imperial College, August 1979.
[8] D. A. Robb, "User's guide to program modent," Tech. Rep., Department of Mechanical Engineering, Imperial College of Science and Technology.
[9] H. P. Yin and D. Duhamel, "Subtraction technique and finite difference formulas for modal parameter estimation." *Mechanical Systems and Signal Processing*, vol. 18, (2004) 1497–1503.
[10] Jerry H. Ginsberg, Matthew S. Allen, A. Ferri, and Chris Moloney, "A general linear least squares SDOF algorithm for identifying eigenvalues and residues," in *21st International Modal Analysis Conference (IMAC-21)*, Orlando, Florida, 2003.
[11] Michael V. Drexel and Jerry H. Ginsberg, "Modal parameter identification using state space mode isolation," in *19th International Modal Analysis Conference (IMAC-19)*, Orlando, FL, 2001.
[12] Michael V. Drexel, Jerry H. Ginsberg, and Bassem R. Zaki, "State space implementation of the algorithm of mode isolation," *Journal of Vibration and Acoustics*, vol. 125, no. April, pp. 205–213, 2003.
[13] Jerry H. Ginsberg, Bassem R. Zaki, and Michael V. Drexel, "Application of the mode isolation algorithm to the identification of a complex structure," in *20th International Modal Analysis Conference (IMAC-20)*, Los Angeles, CA, 2002, pp. 794–801.
[14] Jerry H. Ginsberg and Matthew S. Allen, "Recent improvements of the algorithm of mode isolation," in *Proceedings of IMECE'03, ASME International Mechanical Engineering Congress and Exposition, NCA*, Washington, DC, 2003.
[15] Jerry H. Ginsberg and Matthew S. Allen, "A linear least-squares version of the algorithm of mode isolation for identifying modal properties. part I: Conceptual development," *Journal of the Acoustical Society of America (JASA)*, vol. 116, no. 2, pp. 607–615, 2004.
[16] Matthew S. Allen and Jerry H. Ginsberg, "Modal Identification of the Z24 Bridge Using MIMO-AMI," in *23rd International Modal Analysis Conference (IMAC XXIII)*, Orlando, Florida, 2005.
[17] Randall J. Allemang, *Vibrations Course Notes*, http://www.sdrl.uc.edu/, Cincinnati, 1999.
[18] R. Pintelon and J. Schoukens, *System Identification: a frequency domain approach*, IEEE Press, Piscataway, NJ, 2001.
[19] Jerry H. Ginsberg, *Mechanical and Structural Vibrations*, John Wiley and Sons, New York, first edition, 2001.
[20] Mircea Rades, "A comparison of some mode indicator functions," *Mechanical Systems and Signal Processing*, vol. 8, no. 4, pp. 459–474, 1994.
[21] Herman Van Der Auweraer and J. Leuridan, "Multiple input orthogonal polynomial parameter estimation," *Mechanical Systems and Signal Processing*, vol. 1, no. 3, pp. 259–272, 1987.
[22] Herman Van Der Auweraer, Patrick Guillame, Peter Verboven, and S. Vanlaunduit, "Application of a fast-stabilizing frequency domain parameter estimation method," *Journal of Dynamic Systems, Measurement, and Control*, vol. 123, pp. 651–658, 2001.
[23] Patrick Guillame, Peter Verboven, S. Vanlaunduit, Herman Van Der Auweraer, and Bart Peeters, "A poly-reference implementation of the least-squares complex frequency-domain estimator," in *International Modal Analysis Conference (IMAC XXI)*, Kissimmee, Florida, 2003.
[24] Randall J. Allemang and D. L. Brown, "A unified matrix polynomial approach to modal identification," *Journal of Sound and Vibration*, vol. 211, no. 3, pp. 301–322.
[25] Peter Van Overschee and Bart De Moor, "Continuous-time frequency domain subspace system identification," *Signal Processing*, vol. 52, pp. 179–194, 1996.
[26] Peter Van Overschee and Bart De Moor, *Subspace Identification for Linear Systems: Theory-Implementation-Applications*, Kluwer Academic Publishers, Boston, 1996.
[27] Katrien De Cock, Bart Peeters, Antonio Vecchio, Bart De Moor, and Herman Van Der Auweraer, "Subspace system identification for mechanical engineering," in *Proceedings of ISMA2002 - International Conference on Noise and Vibration Engineering*, Leuven, Belgium, 2002, vol. III, pp. 1333–1352.
[28] S. Marchesiello, B.A.D. Piombo, and S. Sorrentino, "Application of the CVA-BR method to the Z24 bridge vibration data," in *19th International Modal Analysis Conference*, Kissimmee, Florida, 2001.
[29] Bart Peeters, Patrick Guillame, Herman Van Der Auweraer, B. Cauberghe, Peter Verboven, and Jan Leuridan, "Automotive and aerospace applications of the polymax modal parameter estimation method," in *International Modal Analysis Conference (IMAC XXII)*, Dearborne, Michigan, 2004.
[30] B. Cauberghe, Patrick Guillame, Peter Verboven, Eli Parloo, and Steve Vanlanduit, "A poly-reference implementation of

the maximum likelihood complex frequency-domain estimator and some industrial applications," in *22nd International Modal Analysis Conference (IMAC XXII)*, Dearborn, Michigan, 2004.